**TECHNICAL ARTICLE**

# Effect of Applied Energy on the Microstructure, Texture, and Mechanical Properties of Short-Circuit Metal Inert Gas-Welded Modified Cr-Mo Steel Joints

**S. Madhavan[1] · M. Kamaraj[2] · B. Arivazhagan[3]**

## Abstract

Modified 9Cr-1Mo is a ferritic-martensitic steel widely used in steam generators of fast breeder reactors in the nuclear industry due to their enhanced creep resistance. In the present investigation, P91 steel was welded without preheat using three different heat inputs by pulsed short-circuit metal inert gas welding process using a ER90S-B9 wire electrode for the first time. The microstructural developments were characterized by using optical and electron microscopy, while the residual stresses were measured by X-ray diffraction using the $\sin^2\psi$ method. The grain size variation in the fusion zone/heat-affected zone was effectively studied using electron backscattered diffraction to bring out the changes quantitatively. The weld zone had a consistent texture, while the heat-affected zone was random. The grain size tends to increase with the increase in heat input which leads to reduced joint strength. It is evident that at highest heat input, the weld microstructure shows substantial precipitation of $M_{23}C_6$-type carbides. The residual stresses were near compressive in the weld-HAZ, while maximum tensile stresses were found for the highest heat input.

**Keywords** 9Cr-1Mo steel · Microstructure · Texture · Joint strength · Residual stress

## Introduction

High-Cr (9–12% Cr) ferritic steels also known as ferritic-martensitic (F-M steels) are used in ultra-supercritical (USC) thermal power plants, fast breeder reactors (FBR) and prototype—FBRs in the nuclear industry [1, 2]. Among the high-Cr ferritic steels, P91 steel is widely used. These steels are developed from plain 9Cr-1Mo (P91) steel by adding strong carbonitride-forming elements such as V, Nb, and N to enhance the service temperatures up to 600 °C. The carbonitrides present within the lath martensite effectively block the dislocation movement, thereby improving the creep strength. P91 steel possesses excellent weldability, but sufficient precautions must be followed to ensure production of defect-free weldments [2, 7]. Insufficient heat input and poor post-weld heat treatments result in cracks, subsequently leading to catastrophic failure in the real-time scenario.

Various welding processes used in joining of P91 steel are gas tungsten arc welding (GTAW), flux-cored arc welding (FCAW), and metal-cored arc welding (MCW). The welding of these steels by low heat input process like gas metal arc welding (GMAW) and high heat input process like submerged arc welding (SAW) is quite common in fabrication industries [12]. The latter process results in wider heat-affected zone (HAZ), thereby reducing the creep strength. There are various issues associated with welding of P91 steels; some of them are poor strength in case of flux-shielded processes like FCAW, SAW, and formation of δ ferrite in the weld that originates due to the presence of chromium and silicon. The steel is also prone to cold cracking due to high alloy content and martensite formation. These issues are overcome by providing a suitable preheat (200 °C) and interpass temperature (in case of multipass welding). It is also mandatory to keep the preheating temperature below the martensitic finish ($M_f$) temperature to

✉ S. Madhavan
madhavan.tes@gmail.com

1 Department of Mechanical Engineering, SRM Institute of Science and Technology, Kattankulathur, Chennai 603203, India

2 Department of Metallurgical and Materials Engineering, Indian Institute of Technology Madras, Chennai 600036, India

3 Materials Development and Technology Division, Indira Gandhi Centre for Atomic Research, Kalpakkam 603 102, India

complete the transformation after welding. Sufficient interpass temperature prevents hydrogen pick up into the welds. Furthermore, a threshold temperature of 370 °C is suggested to avoid solidification cracking [3–6]. GTA welding of P91 steel has better weld strength, but the process has limited productivity. However, with the development of A-GTAW (activated flux-gas tungsten arc welding) process, the weld zone showed the presence of δ ferrite [7]. Power beam processes, like laser and electron beam welding, are increasingly used to join P91 steels. These processes increase the life of the weldment by minimizing the HAZ due to highly localized heating, thereby enhancing the creep strength of the joints. Laser welding of P91 steel generally provides quality welded joints, but the formation of δ ferrite is a serious issue [8]. Rapid solidification with reduced heat input can minimize HAZ grain coarsening, thereby inhibiting type IV cracking in service.

GMAW of P91 steels resulted in lack of fusion and oxide inclusions with wire electrodes [9]. The same can be reduced using a metal-cored wire process. Electron beam welding resulted in high tensile residual stress in the region susceptible to type IV cracking [10, 11]. Pulsed-GMAW is found to benefit in terms of high deposition rate and accurate control of heat input over conventional GMAW [12–14]. In comparison with other conventional processes, P-GMAW reduces HAZ width and facilitates promising weld microstructure and properties [15, 16].

Sound joints with minimal heat inputs are produced using solid-state welding processes. However, there are restrictions arising from intricate shapes and sizes. It is now mandatory to have a fusion welding technique with minimal cost for joining materials with lowest possible heat input. At this juncture, a recent development called the cold metal transfer (CMT) welding which is the short-circuit metal transfer process is found to be ideal. Compared to P-GMAW, GTAW, and laser weld brazing, CMT process makes use of a simple metal transfer mechanism (reciprocating motion of wire). Thus, CMT is the ideal candidate due to reduced heat input, enhanced welding speed, and equipment size.

Keeping in mind the above facts, it is evident that limited research has been reported on the use of pulsed-cold metal transfer (P-CMT) welding for Cr-Mo steels. In this study, varying heat inputs are used to produce the welds. Microstructure and precipitates in these welds are characterized using transmission electron microscopy (TEM). Variation in grain sizes was effectively studied by electron backscattered diffraction to reveal the changes quantitatively in the weld and heat-affected zone. Mechanical properties including tensile strength, hardness, and residual stresses are correlated with microstructural features.

## Experimental Work

### Materials

In the present study, P91 steel as per ASTM specification A335 M-11 in the normalized (1080 °C-1 h) and tempered (760 °C-2 h) condition was used as the base material. Solid wire of 1.2 mm diameter was used as the filler metal (AWS ER90S-B9) in the preparation of weldments. The nominal composition of the filler and base metal is given in Table 1.

### Experimental Procedure

As-received P91 steel was cut into size of 130 mm×40 mm×3 mm suitable for welding. The plates were welded in the flat butt configuration by P-CMT process, while the welding location was cleaned with acetone. Cross-weld tensile test samples (gauge length 30 mm; gauge width 6 mm; overall length 100 mm) were cut according to AWS B4-16 standard. For the sake of clarity, the heat inputs are designated as A, B, and C. Welding parameters used to obtain heat inputs of A, B, and C are shown in Table 2. Commercially available 82% Ar-18% $CO_2$ was used as the shielding gas with a flow rate of 22 lpm. The heat input is calculated by using a digitized oscilloscope to record the current and voltage measured between the work material and the torch tip. The mean values were reported after several trails from the recorded waveforms subsequently used in Eq 1 to determine the heat input (J mm$^{-1}$).

$$\text{Heat Input, } Q = \frac{\eta \times V \times I \times 60}{S \times 1000} \tag{1}$$

**Table 2** Welding parameters used to obtain designated heat inputs

| Sample description | Current ($I$) | Voltage ($V$) | Speed (mm min$^{-1}$) | Heat input (J mm$^{-1}$) |
|---|---|---|---|---|
| A | 100 | 17.3 | 228.6 | 360 |
| B | 105 | 17.5 | 254.0 | 345 |
| C | 110 | 17.7 | 279.4 | 330 |

**Table 1** Nominal composition of P91 steel and weld (wt%)

| Materials | C | Cr | Mo | Si | Mn | V | S | P | Ni | Nb |
|---|---|---|---|---|---|---|---|---|---|---|
| P91 | 0.12 | 9.13 | 0.86 | 0.27 | 0.42 | 0.22 | 0.02 | 0.02 | 0.22 | 0.06 |
| Weld | 0.09 | 8.75 | 1.08 | 0.2 | 1.0 | 0.19 | 0.01 | 0.01 | 0.75 | 0.05 |

where $V$ = voltage in Volts, $I$ = current in Amps, $S$ = welding speed in mm min$^{-1}$, and the arc efficiency $\eta = 0.8$.

Standard metallographic procedures were followed for microstructural observations. Cross sections of the weld were cut, and the specimens were polished. Villella's reagent (1 g picric acid + 5 ml HCl acid and 100 ml ethanol) was used to etch the specimens to reveal the microstructure. The specimens were observed under optical microscopy and transmission electron microscopy to study the effect of heat input on the microstructural features of the weld. Colloidal silica was used in the preparation of samples for the texture analysis. Microhardness survey was carried out across the weld with a Shimadzu hardness tester at a load of 500 g at regular intervals of 0.2 mm. Cross-weld tensile test samples were cut out from the defect-free joints and were tested on a 30kN INSTRON machine at a constant loading rate of 0.5 mm/min.

Residual stresses in the transverse direction were measured as they contribute to the structural integrity of the weld. Therefore, residual stresses were measured by the $\sin^2\psi$ side inclination method. The peak search was carried out using full width half maxima (FWHM) technique using Cr-K$\alpha$ radiation in a RIGAKU X-ray diffractometer, equipped with a beam size of 1.5 mm × 1.5 mm at 18 mA and 30 kV with a step size of 0.2° and 1 mm spot size. The diffracted rays were measured at different angles (tilt angle, $\psi = 0$–45) by fixing a diffraction plane of (211) for Cr-Mo steels. Lattice constant of $A = 1.064$, Poisson's ratio of 0.28, and diffraction constant of 75 GPa were taken. Approximately 5 points were measured on the weld and 10 points on either side. The effect of variation in heat input on the variation in microstructure of the weld, texture, strength, and residual stress was analyzed.

## Results and Discussion

### Radiographic Qualification of Weldments

After welding, $^{192}$Ir $\gamma$-ray examination was conducted to assess the quality of the weld. ASTM No: 10-hole-type penetrometer was used, and the sensitivity was calculated as per 1T which is clearly visible. The weld bead was fully exposed with an exposure time, and source-to-film (SFD) distance was fixed as 2 min and 30 s and 50 inches by trial and error method using the single-wall single-image (SWSI) technique. Figure 1 shows the radiographic image of the P91 steel weld produced by P-CMT process. The weldment is free from spatter, lack of fusion, and weld discontinuity. The weld is qualified as it meets the ASTM reference radiograph standard and can be accepted.
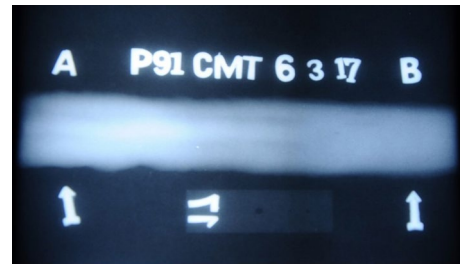


**Fig. 1** Radiographic image P91 steel joint produced by P-CMT process

## Microstructures of Weld and HAZ

### Base Metal

The scanning electron microscopy image of the P91 steel consists of typical lath martensite structure with carbides distributed along prior austenite grain boundaries (PAGBs) and laths (Fig. 2). The base metal is free from $\delta$-ferrite since it is cooled under equilibrium conditions. The lath martensite structure has high dislocation density. Post-weld tempering results in two kinds of precipitates the first being $M_{23}C_6$ carbides located at PAGBs and finely dispersed MX-type carbonitrides within laths. The major precipitates observed in base metal are $M_{23}C_6$ with few MX carbonitride precipitates within the interior of martensite [17, 18].

### Weld

The weld metal begins to solidify as $\delta$-ferrite at 1505 °C and attains saturation at 1424 °C. Between 1506 °C and 1430 °C, only $\delta$-ferrite is present and it begins to transform to $\gamma$ from 1421 °C. The transformation of $\delta$ to $\gamma$ tends to linger till the weld cools down to 738 °C, the threshold temperature beyond which $\gamma$ is fully stable. The complete transformation of $\delta$-ferrite to austenite depends on the time spent by the weld metal in $\delta + \gamma$ and $\gamma$ phase fields. Volume fraction of $\delta$-ferrite retained in the weld is less when the residence time of weld spent in the two-phase fields (duplex field) is high. Volume fraction of the $\delta$-ferrite in the weld metal decreases with the solidification rates experienced [19]. In the current study, as the heat input increased, the $\delta$-ferrite content in the weld also increased. The peak temperature increases with the increase in heat input. The highest heat input causes an increase in peak temperature and more time spent in duplex field than the lowest heat input.

As the time spent is more at high heat input, more nucleation and growth of delta ferrite are possible and the retained $\delta$-ferrite is more due to rapid cooling rate. Hence, the $\delta$-ferrite is more in weld produced using highest heat input. At low heat input, the peak temperature is low so

there may not be sufficient time to be spent in duplex field for the nucleation and growth of δ-ferrite and hence low volume fraction of δ-ferrite was observed. This is evident from the microstructure as shown in Fig. 3. In the current study, the heat input observed is not sufficient to facilitate complete transformation of δ-ferrite to austenite. This indicates that it would be difficult to avoid δ-ferrite in the P-CMT weld metal of P91 steel, though its content can be decreased with the reduction in the heat input. Among the precipitates, $M_{23}C_6$ content was found to be highest

and its volume fraction is 0.019. The $M_{23}C_6$ dissolves at a temperature of 863 °C.

The optical micrograph (Fig. 3a) of the weld zone produced at 330 J/mm, and the respective HAZs shows transformation of martensite and large patches of ferrite, probably due to low heat input retaining the partially melted ferrite. The HAZ shows fine islands of ferrite. For the heat input of 345 J/mm (Fig. 3b), there is complete transformation of martensite with the least precipitation of carbide which resulted in the high joint strength. The
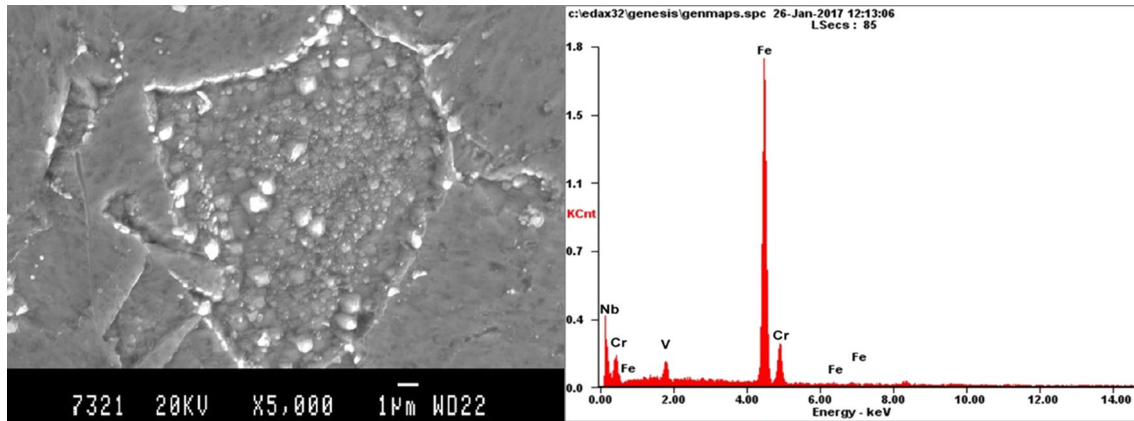


**Fig. 2** Scanning electron microscopy micrograph of the as-received P91 steel and EDS spectrum of $M_{23}C_6$ carbides
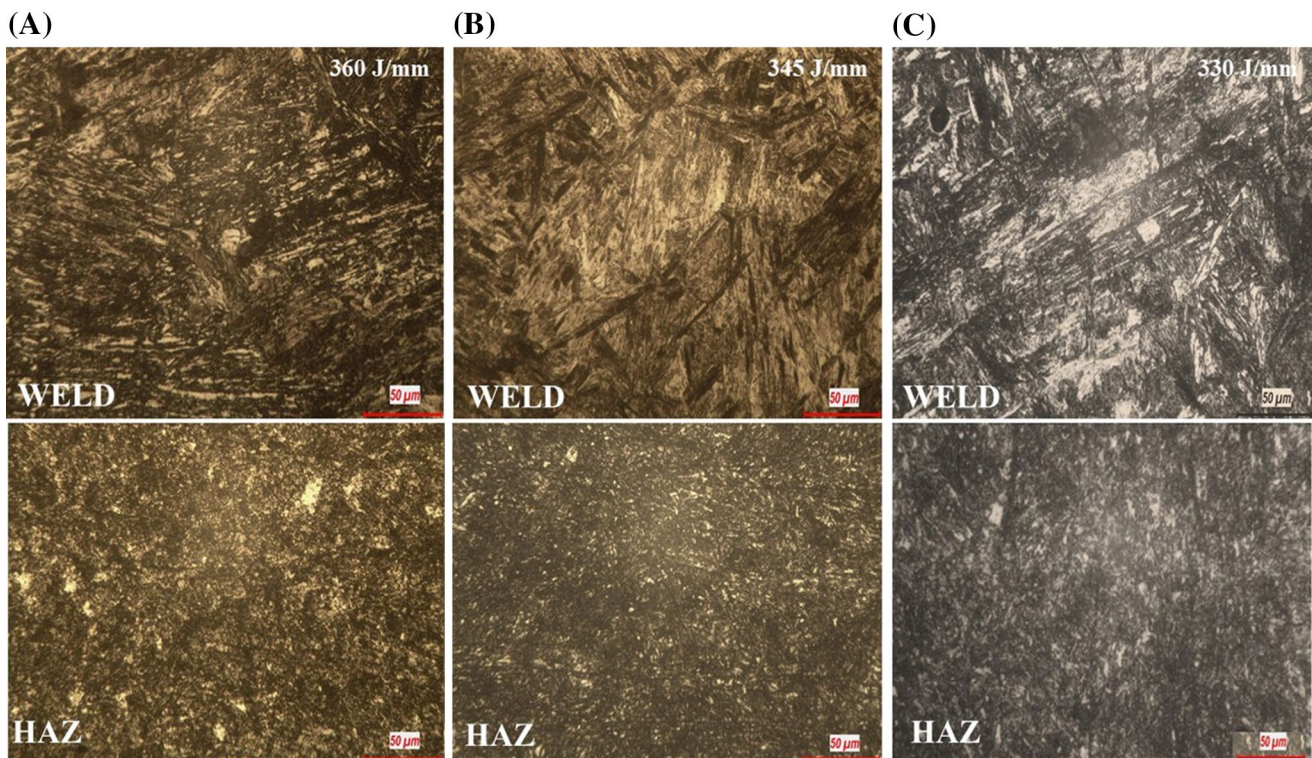


**Fig. 3** Optical images of the weld and HAZ for heat inputs of (**a**) 360 J/mm, (**b**) 345 J/mm, and (**c**) 330 J/mm

HAZ shows low carbide precipitation with untransformed ferrite, whereas when the heat input increases (360 J/mm), precipitation of carbide is maximum which reduces the strength of the welded joint (Fig. 3c).

At 330 J/mm it is found that there is formation of a Y-junction and coarsening of the martensite (Fig. 4c). A localized clustering of two neighboring lath boundaries, with low-angle misorientations, leads to negligible decrease in the dislocation density. These lath boundaries usually can migrate with the rise in heat input primarily due to reorganization of dislocations. This results in reduction in elastic strain which could be the reason for degradation in strength. This also results in softening. Furthermore, structure of the lath boundaries and the presence of carbides are also responsible for the decrease in the strength.

Volume fraction of carbides and carbonitrides increases with increasing heat input (360 J/mm), but size and morphology of the carbides tend to change because of the jerky motion provided by the process. At 360 J/mm the needle particles are responsible for the decrease in the tensile ductility due to early fracture at room and elevated temperatures (Fig. 4a). At a low heat input, there is partial dissolution and coagulation of these precipitates which also could result in enhanced strength. The fraction of globular carbides tends to decrease with the increase in heat input. Within the ferritic matrix, these precipitates nucleate and contribute significantly to the strength. It is also noted that carbides are clearly visible along the boundaries with sizes ranging from 50 to 80 nm. The $M_{23}C_6$ carbides exhibiting the globular shape are observed only for the intermediate heat input of 345 J/mm (Fig. 4b). Optimum heat input results in the formation of globular precipitates which is crucial to achieve enhanced mechanical properties. High resistance to coarsening of the carbides is attributed to the presence of tungsten.

## Texture Analysis of Weldments

Optical microscopy provides approximate evaluation of the microstructure after welding because of the complexity in differentiating the orientation of grains and phases. Due to random solidification, the grain sizes vary arbitrarily. To distinguish and to substantiate the microstructure (weld zone and HAZ), electron back scatter diffraction (EBSD) is used in the present study. Effect of variation in heat input on the microstructural changes is critically examined and reported. Figure 5 shows the inverse pole figure (IPF) for the weld zone and HAZ. All grains with the same color codes correspond to the identical orientation.

The average grain size at heat input of 360 J/mm was measured in the weld, and the HAZ was found to be ~ 30 μm and ~ 75 μm, respectively. The joint strength was poor at this heat input since the grain sizes are very large. For all the heat inputs, the HAZ grains had a random orientation, whereas in the weld zone they tend to grow directionally. This generally alters the mechanical properties of the material. At a heat input of 345 J/mm, the average grain size in the weld zone was ~ 15 μm and ~ 25 μm in the HAZ. Annealing twins as seen in Fig. 5c are not lenticular, and their shapes are found to vary since there is no deformation associated with their formation. These twins are formed because of grain boundary migration and recrystallization [20]. The shapes of these twins have a vital role in fixing the interfacial energy and minimizing the same [19]. With the reduction in the heat input to 330 J/mm, twins are still visible near the interface with a HAZ and weld zone grain sizes of ~ 35 μm and ~ 15 μm.
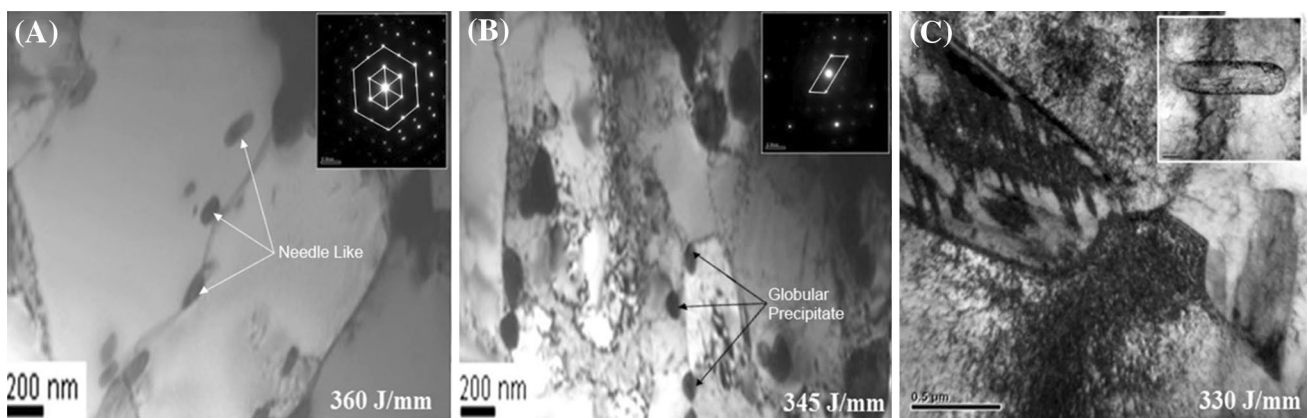


**Fig. 4** Transmission electron microscopy micrograph of the weld zone at (**a**) 360 J/mm with needle-like (film-like) precipitates, (**b**) 345 J/mm with globular precipitates present at the grain boundaries, (**c**) 330 J/mm showing triple point of prior austenite grains with lath martensite. Inset shows SAED patterns of needle-like and globular precipitates

**Fig. 5** IPF of the HAZ and weld zone for heat inputs of (**a**) 360 J/mm, (**b**) 345 J/mm, and (**c**) 330 J/mm
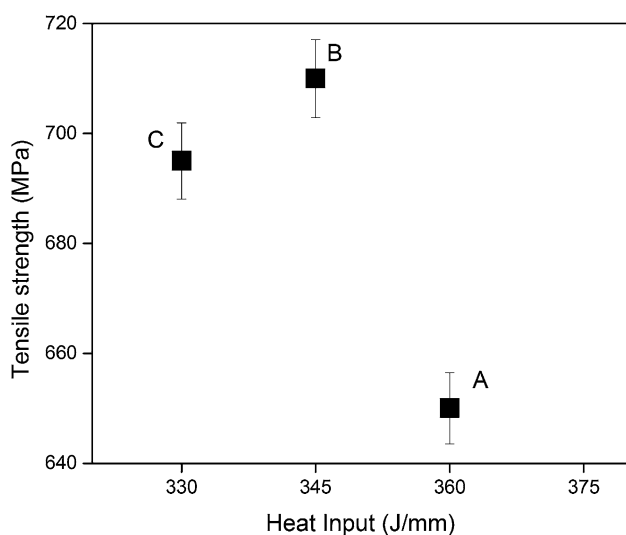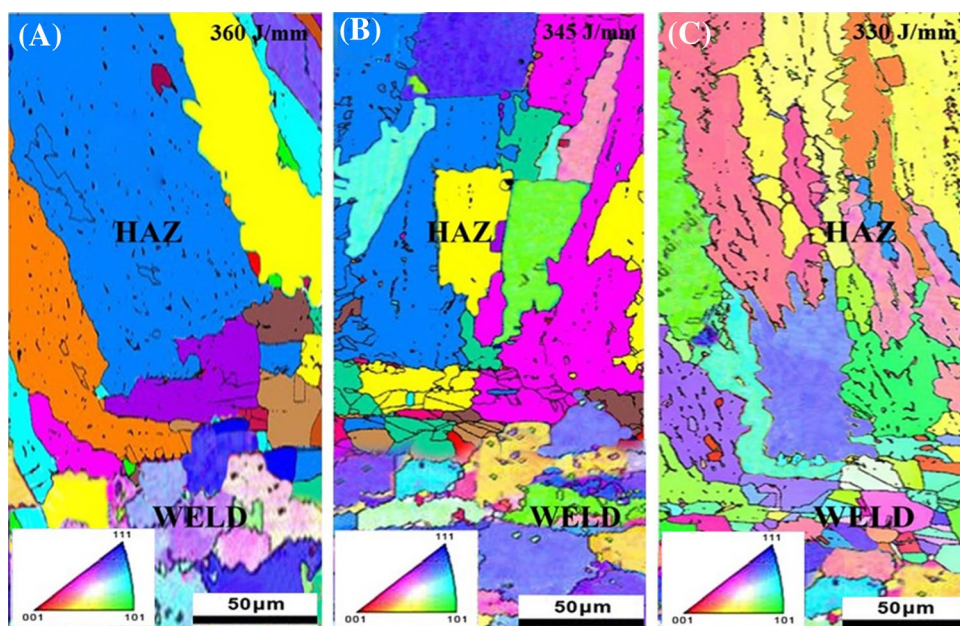


**Fig. 6** Tensile strength at the designated heat inputs of (**a**) 360 J/mm, (**b**) 345 J/mm, (**c**) 330 J/mm



In the current investigation, ferritescope was used to determine the ferrite number (FN) for all the heat inputs. The ferrite content in the weld zone reduced with the reduction in the heat input from 2.43 to 0.65%.

## Mechanical Properties

The tensile strength of P91 steel joints obtained with different heat inputs by P-CMT process is given in Fig. 6. The welds made with heat input of 345 J/mm have the highest tensile strength of 710 MPa. When the heat input is lower, dilution is low and hence the volume of strengthening precipitates dissolving into the weld is also minimal. When the heat input is increased, the grains in the heat-affected zone get coarsened and the dendrites in the weld increase, thereby degrading the joint strength. This is also evident from the microstructural observations. The variation in tensile strength shown could be due to the agglomeration of precipitates which is evidently more in the 360 J/mm, whereas at 345 J/mm the precipitates pin the grain boundaries inhibiting the grain growth. The variation in heat inputs had significant effects on the microstructural characteristics of the joints (Fig. 5a–c). Hence, suitable heat inputs must be determined to enhance the joint strength.

Hardness survey is carried out on the weld for all the heat inputs. Figure 7 shows the variation of the ferrite number (FN) and weld zone hardness with respect to change in the heat input. The FN is a volumetric measure to quantify the ferrite content, whereas other qualitative techniques report only the localized area fraction. So, the combinations of these techniques give us an idea about the trend as a function of heat input. At a heat input of 330 J/mm, it was found that the FN content was 3FN with hardness of 550 HV. In the present study, there are two factors considered that affect the hardness of weld. They are precipitate and δ-ferrite content. At the lowest heat input (330 J/mm) due to low ferrite and precipitate content (3FN), the hardness of 550 HV was observed. At a heat input of 345 J/mm despite the δ-ferrite content of 5.8FN, high hardness of 590HV was observed due to the increase in quantity of precipitates. At the highest input of 360 J/mm, δ-ferrite content is more dominant than precipitate content. Hence, the lowest value of 520HV was observed. To conclude with the increase in heat input,
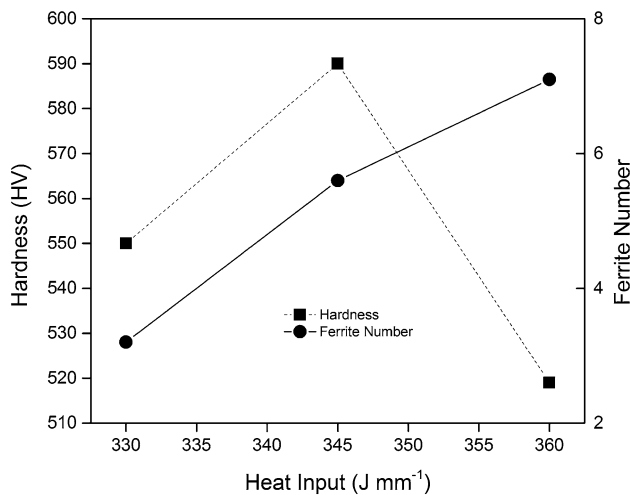
**Fig. 7** Hardness of weld zone and ferrite number at different heat inputs



**Fig. 8** Variation of residual stress across the weld at different heat inputs

δ-ferrite content in weld increases thereby decreasing the hardness of weld. The reduction in hardness is not only due to δ-ferrite content but also due to precipitate content and grain coarsening. Ideal combination to achieve the maximum strength would be 345 J/mm.

## Residual Stress

Residual stresses are stresses that exist independent of restraint. Welding process introduces stresses through thermal expansion or contraction and allotropic transformations. Fine grain heat-affected zone (FGHAZ) interface near the fusion zone exhibited compressive state of stress. For heat input ($B = 345$ J/mm) the tensile stresses are at the minimum, which gave rise to a high tensile strength (710 MPa). The top surface of the weld is exposed to outside so convection, and radiation losses will be more. Therefore, thermal shrinkage on the top surface will be predominant. The material interior which is at an elevated temperature tries to resist the material above so the tensile surface stresses. Stresses are tensile in nature in the HAZ, while the base metals exhibit compressive state of stress. It is obvious that magnitude of residual stresses depends on the heat input.

Since there is a tensile residual stress, the extra stress needed to reach the fracture stress will be less. Hence, the tensile strength decreases with increasing tensile surface residual stress. In P91 steel joints, both sides melt and as the weld solidify, there will be significant contraction. This will be resisted by the base metals, which will pull it back on either side. Hence, there are compressive stresses at the FGHAZ interface for all experimental conditions. Since, the weld is in force equilibrium. There is compressive residual stress present at the interface. This must be balanced by the presence of a tensile residual stress elsewhere (in coarse
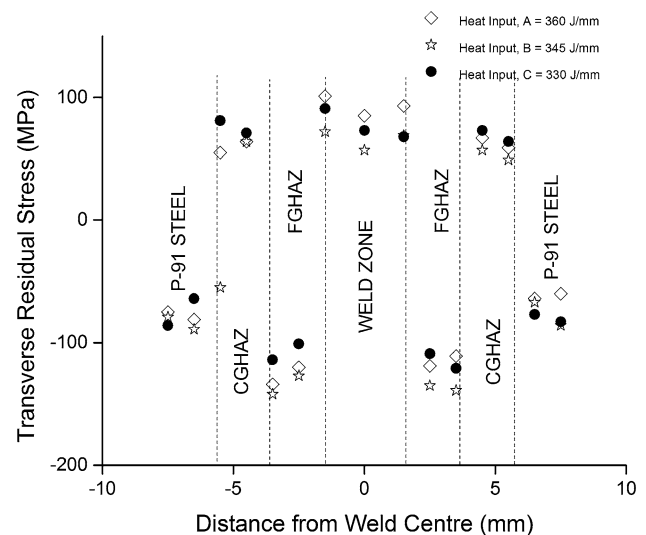
grain heat-affected zone (CGHAZ) and weld zone; a consequence of the welding process) so that the net force on the system is zero. The reduction in tensile strength for the heat inputs (A&C) is due to the variation in stress levels (Fig. 8).

## Failure Modes

Failure modes of welds produced by P-CMT process were determined by visual examination. Tensile loading resulted in failure at CGHAZ is shown in Fig. 9. The cleavage surface surrounded by a pit like area discloses that the fissure is quasi-cleavage. All slant fracture surfaces formed are created by shear rupture and not by pure shear. Shear rupture is identified by elongated or parabolically shaped dimples that point in the direction of shear mating fracture surfaces [21]. The shape of these pits depends on the fraction of micro voids. This failure mode has ductile fracture characteristics with small size dimples and clustering of voids with a stepped appearance.

## Conclusions

P-CMT-welded P91 steels were successfully produced. The effect of varying heat input on the microstructure of the weld, tensile strength of the joints, residual stress, and fracture modes are analyzed. From this investigation, the following important conclusions have been drawn.

- For the range of heat inputs used, welds produced using heat input 345 J/mm had the highest strength. At the
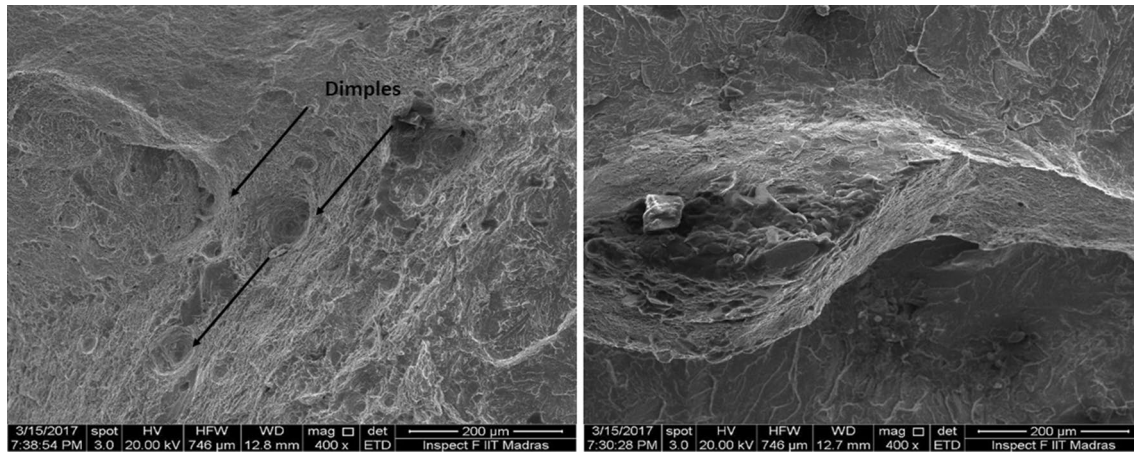
**Fig. 9** HAZ failure of P-CMT-welded P91 steel with small dimples and stepped fracture appearance

highest heat input, the strength was the least due to high δ-ferrite content with coarse precipitates in weld region.

- Texture analysis revealed that for all the heat inputs, HAZ grains had a random orientation, whereas in the weld zone they tend to grow directionally. So, grain growth and orientation can be controlled by governing the heat input which generally alters the mechanical properties of the material. Apart from the texture, the variation in the properties is also due to grain sizes, agglomeration of precipitates, and magnitude of stress.

- FGHAZ near the fusion zone exhibited compressive state of stress, while the weld exhibits tensile stress due to large temperature difference resulting out of heat losses.

- Failure mode has ductile fracture characteristics with small size pits and clustering of voids with a stepped appearance. Preheat free welding carried out at lower heat inputs compared to other fusion welding processes does not result in any kind of cracking. So, P-CMT process can be recommended for welding of Cr-Mo steels.

# References

1. J. Xue, C. Zhou, J. Peng, Creep stress analyses affected by defect geometries on P91 pipe with local wall thinning under high temperature. In: 18th International Conference on Nuclear Engineering, vol. 5. ASME Proceedings; 2010, pp. 523–528
2. J. Blach, L. Falat, P. Ševc, Fracture characteristics of thermally exposed 9Cr-1Mo steel after tensile and impact testing at room temperature. Eng. Fail. Anal. **16**, 1397–1403 (2009)
3. J.A. Francis, G.M.D. Cantin, W. Mazur et al., Effects of weld preheat temperature and heat input on type IV failure. Sci. Technol. Weld. Join. **14**(5), 436–442 (2009)
4. K.K. Coleman, W.F. Newell, P91 and beyond. Weld. J. **86**, 29–33 (2007)
5. S.S.M. Tavares, J.M. Pardal, G.C. Souza et al., Study of cracks in the weld metal joint of P91 steel of a super heater steam pipe. Eng. Fail. Anal. **56**, 464–473 (2015)
6. M. Kondo, M. Tabuchi, S. Tsukamoto et al., Suppressing type IV failure via modification of heat affected zone microstructures using high boron content in 9Cr heat resistant steel welded joints. Sci. Technol. Weld. Join. **11**, 216–223 (2006)
7. B. Arivazhagan, M. Vasudevan, A comparative study on the effect of GTAW processes on the microstructure and mechanical properties of P91 steel weld joints. J. Manuf. Process. **16**, 305–311 (2014)
8. B. Shanmugarajan, G. Padmanabham, H. Kumar et al., Autogenous laser welding investigations on modified 9Cr-1Mo (P91) steel. Sci. Technol. Weld. Join. **16**, 528–534 (2011)
9. W.F. Newell, *Guidelines for Welding P91* (W.F. Newell & Associates, Mooresville, 1991)
10. A. Kundu, P.J. Bouchard, S. Kumar et al., Residual stresses in P91 steel electron beam welds. Sci. Technol. Weld. Join. **18**, 70–75 (2013)
11. J.A. Francis, W. Mazur, H.K.D.H. Bhadeshia, Type IV cracking in ferritic power plant steels. Sci. Technol. Weld. Join. **22**, 1387–1395 (2006)
12. P.K. Ghosh, S.R. Gupta, A.K. Pramanick, Effect of pulse current on shrinkage stress and distortion in multipass GMA welds of different groove sizes. Weld. J. **89**, 43–53 (2010)
13. P.K. Ghosh, K. Devakumaran, H.S. Randhawa, Characteristics of a pulsed-current, vertical-up gas metal arc weld in steels. Metall. Mater. Trans. A **31A**, 2247–2259 (2000)
14. S. Krishnan, D.V. Kulkarni, A. De, Probing pulsed current gas metal arc welding for modified 9Cr-1Mo steel. J. Mater. Eng. Perform. **24**, 1462–1470 (2014)
15. K. Devakumaran, P.K. Ghosh, Thermal characteristics of weld and HAZ during pulse current gas metal arc weld bead deposition on HSLA Steel Plate. Mater. Manuf. Process. **25**, 616–630 (2010)
16. P. Kamal, K.P. Surjya, Effect of pulse parameters on weld quality in pulsed gas metal arc welding: a review. J. Mater. Eng. Perform. **20**, 918–931 (2011)
17. K. Sawada, H. Kushima, M. Tabuchi, K. Kimura, Microstructural degradation of Gr.91 steel during creep under low stress. Mater. Charact. **101**, 106–113 (2015)
18. M. Yoshino, Y. Mishima, Y. Toda, H. Kushima, K. Sawada, K. Kimura, Phase equilibrium between austenite and MX carbonitride in a 9Cr-1Mo-V-Nb steel. ISIJ **45**, 107–115 (2005)

19. B. Arivazhagan, G. Srinivasan, S.K. Albert et al., A study on influence of heat input variation on microstructure of reduced activation ferritic martenistic steel weld metal produced by GTAW process. Fusion Eng. Des. **86**, 192–197 (2011)

20. J.E. Burke, The formation of annealing twins. J. Mater. **2**, 1324–1328 (1950)

21. ASM International, *Metals Handbook, Volume 12: Fractography* (ASM International, 1987), pp. 18–20